Geophys. J. Int. (1989) **99**, 321–329

Finite-difference technique for *SH*-waves in 2-D media using irregular grids—application to the seismic response problem

Peter Moczo

Geophysical Institute, Geoscience Research Centre, Slovak Academy of Sciences, Dúbravská cesta, 842 28 *Bratislava, Czechoslovakia*

Accepted 1989 February 8. Received 1989 January 11; in original form 1988 August 22.

SUMMARY

The finite-difference method is applied to compute the seismic response of 2-D inhomogeneous structures for *SH*-waves. A technique is proposed which uses an irregular grid (a rectangular grid with varying grid spacing). A geological structure may be composed of blocks of media inside of which velocity and density vary linearly in horizontal and vertical directions. The technique allows better adjusted modelling of a medium and, in numerical examples presented, yields more efficient computations as compared to those with regular grids. The technique is tested through comparison with a discrete-wavenumber method.

As an example, the seismic response of the sediment-filled Chusal Valley, Garm region, USSR, is computed. The numerical results are compared with observations.

Key words: finite-difference method, irregular grid, sedimentary basin, seismic response, theoretical seismograms.

1 INTRODUCTION

The finite-difference method is a universal tool to solve seismic wave propagation problems. However, the large size of a model (with respect to the predominant wavelength) and a large difference between the maximum and minimum velocity in the model cause enormous computer memory and computational time requirements in many types of problems. This is one of the reasons for the general use of methods, based on ray theory in structural and exploration seismology. In solving problems with significant interference and diffraction phenomena various hybrid methods (e.g. Mikhailenko & Korneev 1984; Kawase 1988) seem to be the most promising at present. Nevertheless, the finite-difference method and efforts to make finite-difference algorithms more effective are still very important. This is because hybrid methods are not universally applicable to arbitrarily complicated structures and, also, because improving the finite-difference algorithms can be useful also for hybrid methods (if they imply finite-differencing).

One possibility to make finite-difference computations more efficient is to use irregular grids. It is known that for *SH*-waves in a 2-D medium sufficiently accurate results can be obtained up to the frequency f_{ac}, if the grid spacing $\Delta\xi$ satisfies the condition

$$f_{ac} = \beta_{min}/(12\Delta\xi),$$

with β_{min} being the minimum velocity in a medium. According to this condition, in a part of the medium with larger velocity β' the same accuracy is obtained with the larger grid spacing

$$\Delta\xi' = (\beta'/\beta_{min})\Delta\xi.$$

Boore (1970) was probably the first who used an irregular grid. Recently, Korn (1987) used it in his frequency domain finite-difference method. They both used irregular vertical spacing in a 1-D medium. Here, the irregular grid is probably used for the first time for modelling a 2-D laterally inhomogeneous medium.

The technique proposed in this paper is applied to the problem of the seismic response of near-surface local geological structures. The finite-difference method (using a regular grid) has been successfully used to solve this problem, e.g. Boore, Larner & Aki (1971) and Zahradník & Hron (1987).

In Section 2 the explicit finite-difference scheme for an irregular rectangular grid is developed. The model of a medium is specified in Section 3. In Section 4 the properties of the irregular grid and the efficiency of the proposed algorithm are shown, using examples of sedimentary basins. The finite-difference seismograms are compared with those computed by the discrete-wavenumber method. In Section 5 *SH*-seismograms and frequency responses for the sediment-filled Chusal Valley, Garm region, USSR, are computed. Theoretical results are compared with observations by King & Tucker (1984). Some aspects of the proposed technique are discussed in Section 6.

2 FINITE-DIFFERENCE SCHEME FOR AN IRREGULAR RECTANGULAR GRID

2.1 Formulation of the problem

Two-dimensional *SH*-wave propagation in a 2-D inhomogeneous medium is considered. Let us denote the

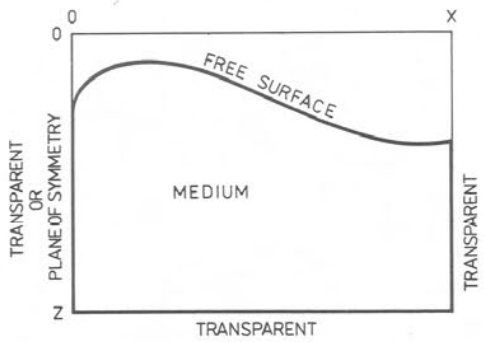

Figure 1. Computational region, medium and types of boundaries.

shear modulus by $\mu(x, z)$, the density by $\rho(x, z)$ and the y-component of the displacement vector by $u(x, z, t)$. The displacement component u satisfies the equation of motion

$$\rho(\partial^2 u/\partial t^2) = \partial(\mu\, \partial u/\partial x)/\partial x + \partial(\mu \partial u/\partial z)/\partial z. \tag{1}$$

The displacement and the velocity are assumed to be zero at the time $t = 0$:

$$u|_{t=0} = 0, \qquad (\partial u/\partial t)|_{t=0} = 0.$$

Let us consider a rectangular computational region where the coordinates x, z are within the boundaries $x \in \langle 0, X\rangle$, $z \in \langle 0, Z\rangle$. X and Z are the extensions of the model in the horizontal and vertical directions. Since we are interested in computing the seismic response of near-surface structures, it is reasonable to consider the boundary conditions shown schematically in Fig. 1. The upper boundary of the medium is the free surface with zero stress. Both the bottom ($z = Z$) and the right ($x = X$) boundary are transparent (non-reflecting). The left boundary ($x = 0$) can be transparent (non-reflecting) or it can represent a plane of symmetry (totally reflecting). Symmetry conditions can only be used in the case of a symmetry of the investigated structure and the wave excitation.

A plane SH-wave, incident on the structure from below, is applied at the line $z = Z_s$, $Z_s < Z$.

The conditions of continuity for the displacement and the stress on the internal interfaces are not explicitly specified, since they are included as a special case of the medium inhomogeneity in the method used below.

2.2 Numerical solution

First, let us cover the computational region by an irregular grid (see Fig. 2) with grid spacings ${}_xh_i$ and ${}_zh_j$ in the x- and z-direction, respectively. The following relations hold:

$${}_xh_i = x_i - x_{i-1}, \qquad i = 2, \ldots, MX, \qquad x_1 = 0,\ {}_xh_1 = 0,$$
$${}_zh_j = z_j - z_{j-1}, \qquad j = 2, \ldots, MZ, \qquad z_1 = 0,\ {}_zh_1 = 0.$$

Besides the grid spacings, let us introduce the quantities ${}_x\bar{h}_i$ and ${}_z\bar{h}_j$ as follows:

$${}_x\bar{h}_i = ({}_xh_i + {}_xh_{i+1})/2,$$
$${}_z\bar{h}_j = ({}_zh_j + {}_zh_{j+1})/2.$$

Further, we denote: Δt as the time spacing, $t_k = (k-1)\,\Delta t$ and $U^k_{i,j}$ as the discrete approximation of displacement $u(x_i, z_j, t_k)$ in the grid point i, j at the kth time level.

To obtain the finite-difference scheme for equation (1),

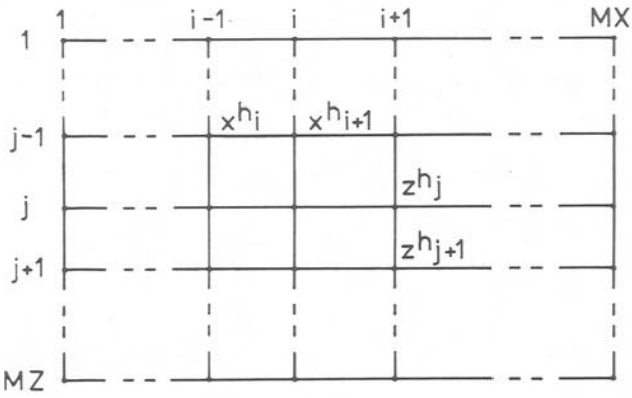

Figure 2. An irregular spatial grid.

we can use two approaches. The so-called 'homogeneous formulation' (or homogeneous media approach) deals with the equation for homogeneous media and explicitly expressed conditions of continuity for the displacement and the stress on the interfaces between media with different elastic parameters. The second approach, the so-called 'heterogeneous formulation' (or heterogeneous media approach) solves directly the equation of motion for heterogeneous media (1) with space dependent coefficients.

Here, we use the 'heterogeneous formulation'. In this, some effective values of the actual shear modulus and the density are determined at the grid points. They measure changes of the actual parameters in a neighbourhood of the grid point. In the approach suggested by Tikhonov and Samarskii (see, e.g. Boore 1972; Mitchell 1969, p. 23; Samarskii 1983), the effective shear moduli are determined as follows:

$$\mu^H_{i,j} = {}_xh_{i+1}\left[\int_{x_i}^{x_{i+1}} dx/\mu(x, z_j)\right]^{-1},$$
$$\mu^V_{i,j} = {}_zh_{j+1}\left[\int_{z_j}^{z_{j+1}} dz/\mu(x_i, z)\right]^{-1}. \tag{2}$$

$\mu^H_{i,j}$ and $\mu^V_{i,j}$ may be called the horizontal and the vertical effective shear modulus, respectively. $\mu^H_{i,j}$ measures how $\mu(x, z)$ changes along the jth grid row between the grid points i, j and $i+1, j$. Similarly, $\mu^V_{i,j}$ measures how $\mu(x, z)$ changes along the ith grid column between the grid points i, j and $i, j+1$.

The discrete approximation of the density $\rho_{i,j}$ in the grid point i, j is determined as follows:

$$\rho_{i,j} = (\rho^{LR}_{i,j} + \rho^{UB}_{i,j})/2,$$
$$\rho^{LR}_{i,j} = (1/{}_x\bar{h}_i)\int_{x_i-({}_xh_i/2)}^{x_i+({}_xh_{i+1}/2)} \rho(x, z_j)\, dx, \tag{3}$$
$$\rho^{UB}_{i,j} = (1/{}_z\bar{h}_j)\int_{z_j-({}_zh_j/2)}^{z_j+({}_zh_{j+1}/2)} \rho(x_i, z)\, dz.$$

The following explicit finite-difference scheme for equation (1) can be obtained

$$\begin{aligned} U^{k+1}_{i,j} = {} & 2U^k_{i,j} - U^{k-1}_{i,j} \\ & + (\Delta t)^2[\mu^H_{i,j}(U^k_{i+1,j} - U^k_{i,j})/{}_xh_{i+1} \\ & - \mu^H_{i-1,j}(U^k_{i,j} - U^k_{i-1,j})/{}_xh_i]/({}_x\bar{h}_i\rho_{i,j}) \\ & + (\Delta t)^2[\mu^V_{i,j}(U^k_{i,j+1} - U^k_{i,j})/{}_zh_{j+1} \\ & - \mu^V_{i,j-1}(U^k_{i,j} - U^k_{i,j-1})/{}_zh_j]/({}_z\bar{h}_j\rho_{i,j}). \end{aligned} \tag{4}$$

Let us remark that in the Soviet literature finite-difference schemes, as for example (4), are called homogeneous schemes, since the same formula holds for all grid points, regardless of whether the point is in a homogeneous region or in the neighbourhood of an interface.

The free surface corresponding to the Earths' surface can be simulated using a zero shear modulus above the surface.

If we suppose ${}_zh_{MZ-1} = {}_zh_{MZ}$, ${}_xh_{MX-1} = {}_xh_{MX}$ and ${}_xh_2 = {}_xh_3$, the formulae derived by Reynolds (1978) can be used to simulate the transparent (non-reflecting) bottom, the right and the left boundary of the computational region, respectively. For example, for the left transparent boundary the formula is:

$$U^{k+1}_{1,j} = U^k_{1,j} + U^k_{2,j} - U^{k-1}_{2,j} - (\Delta t/{}_xh_2)(\mu^H_{1,j}/\rho_{2,j})^{1/2} \times (U^k_{1,j} - U^k_{2,j} - U^{k-1}_{2,j} + U^{k-1}_{3,j}).$$

The formula for the plane of symmetry at the left boundary can be obtained from (4), putting $U^k_{0,j} = U^k_{2,j}$, $\mu^H_{0,j} = \mu^H_{1,j}$ and ${}_xh_1 = {}_xh_2 = {}_x\bar{h}_1$.

To simulate plane wave incidence from below, we use the approach suggested by Alterman & Karal (1968) originally for a point source. For a plane wave the algorithm was used by Virieux (1984). Let us divide our grid into two parts. Part II includes grid rows 1 up to *JOU*, Part I grid rows *JIN* ($=JOU+1$) up to *MZ*. The grid row *JIN* represents the source. It is placed beneath the inhomogeneity (local geological structure). Besides the total field $U_{i,j}$ that is computed in Part II and on the grid row *JIN*, the residual field $R_{i,j}$ is computed in Part I and on the grid row *JOU*. Let $S(t)$ be the time function of the displacement, corresponding to the vertically incident plane wave. Let t_D be the time that the incident wave needs to travel the distance ${}_zh_{JIN}$ from the grid row *JIN* to the grid row *JOU*. Now we can write the scheme of the algorithm. At the first time level $U^1_{i,JIN} = S(0)$ for $i = 1, MX$. All other quantities $U^1_{i,j}$ and $R^1_{i,j}$ are zero. At each further time level during radiating from the source row *JIN*, $U_{i,j}$ and $R_{i,j}$ are computed as follows:

(1) $R^{k+1}_{i,j}$; $j = JIN, MZ$, $i = 1, MX$—using the difference scheme (4) and formulae for the boundaries of the computational region.
(2) $U^{k+1}_{i,JIN} = R^{k+1}_{i,JIN} + S(k\Delta t)$; $i = 1, MX$.
(3) $U^{k+1}_{i,j}$; $j = 2, JOU$, $i = 1, MX$—using the difference scheme (4) and formulae for the boundaries of the computational region.
(4) $R^{k+1}_{i,JOU} = U^{k+1}_{i,JOU} - S(k\Delta t - t_D)$; $i = 1, MX$.

After the radiating finishes, it is possible to formally use the above scheme with zero values of $S(t)$. However, in all computations presented in this paper the following approach is used. After the radiating finishes, the grid is reduced. Only the field $U_{i,j}$ is computed and the grid row *JIN* (or a grid row with a lower index) becomes a new non-reflecting bottom boundary.

It is very important that the above approach to simulate the plane wave incidence allows the use of a fixed number of grid rows in a homogeneous basement beneath the local near-surface inhomogeneity, regardless of the size of grid spacing between the grid rows and regardless of the duration of radiation.

Finally, let us remark that it is not a problem to generalize the above scheme for the case of oblique incidence.

We wish our computation to be sufficiently accurate up to the frequency f_{ac}. In the case of a regular grid we have to use a grid spacing $\Delta\xi$, satisfying the well-known condition $\Delta\xi \leq \beta_{min}/(12f_{ac})$ where β_{min} is the minimum velocity in the medium. According to this condition in each part of the medium the grid spacings ${}_xh_i$ and ${}_zh_j$ should satisfy conditions

$${}_xh_i \leq \beta/(12f_{ac}) \text{ and } {}_zh_j \leq \beta/(12f_{ac}) \quad (5)$$

where β is the local velocity.

According to the known stability condition in the case of a regular spatial grid the time spacing Δt in the case of the irregular grid should satisfy the condition

$$\Delta t \leq (h/\beta)_{min}/\sqrt{2},$$

$(h/\beta)_{min}$ being the minimum ratio of the grid spacing and corresponding local velocity β.

3 SPECIFICATION OF THE MODEL

First, let us consider, for example, a sedimentary basin. Let the velocity be increasing linearly from some value v_1 at the free surface up to v_2 at the basin bottom. The usual way to model the medium in such a case is to use the regular vertical grid spacing and to approximate the continuous velocity–depth distribution by a system of thin horizontal homogeneous layers with thicknesses equal to the grid spacing or to the half of the grid spacing (see Fig. 3a).

Since the velocity increases with depth we can use—according to conditions (5)—an increasing grid spacing. However, using homogeneous layers with thicknesses equal to grid spacings would yield too rough approximation of the continuous velocity–depth distribution (see Fig. 3b). To avoid this problem and to save varying the grid spacing at the same time, we construct the model in such a way that the continuous linear increase of the velocity is strictly taken into account.

Let the velocity and the density along the grid column i between the grid points i, j and $i, j+1$ be linear functions of the z-coordinate:

$$\beta = \beta_0 + \beta_1 z, \qquad \rho = \rho_0 + \rho_1 z.$$

Then the shear modulus μ along the grid column i between the grid points i, j and $i, j+1$ is

$$\mu = (\rho_0 + \rho_1 z)(\beta_0 + \beta_1 z)^2. \quad (6)$$

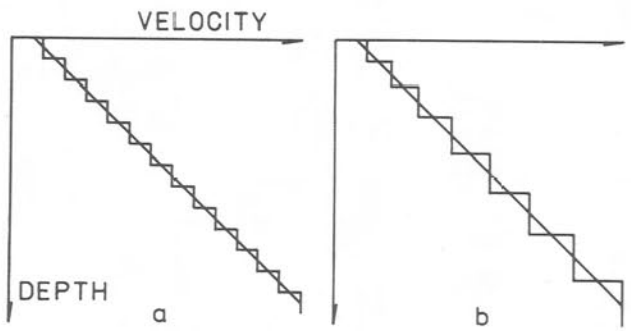

Figure 3. Approximation of a linear velocity–depth distribution by a system of homogeneous layers with thicknesses equal to grid spacings: (a) using an equidistant vertical grid spacing, (b) using a varying grid spacing. The latter approximation would be too rough.

Inserting (6) into (2) yields for $\mu^V_{i,j}$

$$\mu^V_{i,j} = {}_zh_{j+1}\rho_1\beta_1^2(\beta_{01}-\rho_{01})^2 \times \{(\beta_{01}-\rho_{01})[1/(\beta_{01}+z_{j+1}) - 1/(\beta_{01}+z_j)] + \ln|(\rho_{01}+z_{j+1})/(\beta_{01}+z_{j+1})| - \ln|(\rho_{01}+z_j)/(\beta_{01}+z_j)|\}^{-1}, \quad (7)$$

where $\beta_{01}=\beta_0/\beta_1$ and $\rho_{01}=\rho_0/\rho_1$. An analogous formula can be obtained for $\mu^H_{i,j}$, assuming a linearly varying velocity and density along the jth grid row between the grid points i, j and $i+1, j$.

From (3) we obtain for $\rho^{UB}_{i,j}$ the following expression:

$$\rho^{UB}_{i,j} = \rho_0 + \rho_1[z_j + ({}_zh_{j+1} - {}_zh_j)/4]. \quad (8)$$

In fact, this is equivalent to the arithmetical mean value of the density $\rho_0+\rho_1(z_j-{}_zh_j/2)$ at $z_j-{}_zh_j/2$ and the density $\rho_0+\rho_1(z_j+{}_zh_{j+1}/2)$ at $z_j+{}_zh_{j+1}/2$. An analogous formula can be obtained for $\rho^{LR}_{i,j}$.

The formulae (2), (3), (7) and (8) have to be modified, if the interface between two media with different parameters intersects the grid column or the grid row between two grid points. For example, $\mu^V_{i,j}$ is then expressed as follows:

$$\mu^V_{i,j} = {}_zh_{j+1}\left[\int_{z_j}^{z_j+a} dz/\mu^1(x_i, z) + \int_{z_j+a}^{z_{j+1}} dz/\mu^2(x_i, z)\right]^{-1}. \quad (9)$$

Here, the superscripts 1 and 2 correspond to the medium 1 and to the medium 2, respectively; a is the distance from the grid point i, j to the point of intersection of the interface and the grid column i.

A computer program for preparing the grid model (i.e. computing $\mu^V_{i,j}$, $\mu^H_{i,j}$ and $\rho_{i,j}$ in each grid point) has been written that allows the geological structure to be modelled as a combination of blocks of media with different parameters. Inside the block the velocity and the density may be constant or may vary linearly in the horizontal and vertical direction. The geometry of the interfaces between blocks may be arbitrary, i.e. the interface need not cross the grid points.

4 TEST EXAMPLES

To show the properties of the irregular grid, *SH*-seismograms at the free surface of two sedimentary basins are presented. First, a sedimentary basin composed of two homogeneous blocks of media is considered. Second, a sedimentary basin inside of which the velocity linearly increases with depth is taken into account. In both cases, the geometry of the sediment–basement interface is the same as in the classical basin problem studied by Boore *et al.* (1971) and then by many authors (recently in detail by Moczo, Bard & Pšenčík 1987). The sediment–basement interface is given by the formula $z(x) = D + C[1-\cos\{2\pi(|x| - w/2)/w\}]/2$, $-w/2 \leq x \leq w/2$ and $z(x) = D$ elsewhere (see Fig. 4). $D = 1$ km, $C = 5$ km, $w = 50$ km, i.e. the maximum depth at the centre is 6 km and the total width of the basin is 50 km. From above, the basin is bounded by a plane free surface (see Figs 4 and 6).

In both cases a plane *SH*-wave incident vertically from below is taken into account. Due to the symmetry of the problem, only the right half of the basin is considered and the left-hand boundary represents a plane of symmetry in both cases.

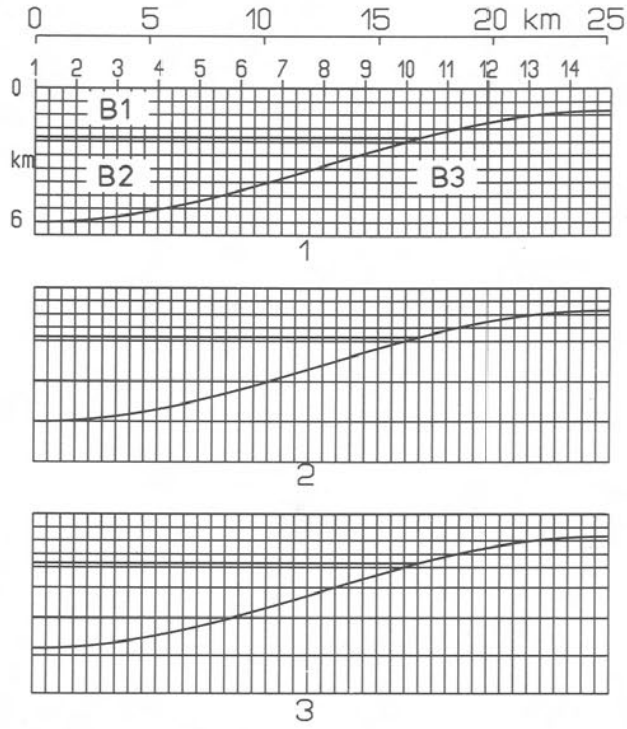

Figure 4. Parts of three grids 1–3 used to compute the response of the same basin, composed of two homogeneous blocks B1 and B2. Grid 1 has a regular grid spacing, grid 2 has an abrupt change in the grid spacing, grid 3 has a gradually increasing grid spacing. Due to the symmetry of the problem the grids only cover the right half of the basin. Numbers 1–14 denote receivers.

4.1 The sedimentary basin composed of two homogeneous blocks

The basin is composed of two blocks B1 and B2 separated by a horizontal interface at 2.2 km depth. The homogeneous basement B3 underlies the basin (see Fig. 4). The parameters of the model are given in Table 1.

The time dependence of the incident wave is given by the Gabor impulse $s(t) = \exp[-\{\omega(t-t_s)/\gamma\}^2]\cos\{\omega(t-t_s)+\psi\}$. Here $\omega = 2\pi f_P$, f_P is the predominant frequency, $t_s = 0.45\gamma/f_P$, and the signal is defined in the interval $\langle 0, 2t_s\rangle$. In the computations $f_P = 0.025$ Hz, $\gamma = 4$ and $\psi = \pi/2$ are used.

The seismograms are computed for three grids 1, 2 and 3 (see Fig. 4). A total of 51 grid columns and an equidistant grid spacing of 600 m in the horizontal direction are used in Grids 1–3. (In Fig. 4 only the 1st to the 42nd grid columns are shown.) Grids 1–3 differ from each other by the grid spacing in the vertical direction and thus by the number of grid points. (Here, let us remind ourselves that the approach used to simulate the wave incidence, see Section 2.2, allows

Table 1. Parameters of the basin shown in Fig. 4.

Block	*S*-wave velocity ($m\,s^{-1}$)	Density ($kg\,m^{-3}$)
B1	400	1700
B2	1200	2200
B3	3500	3300

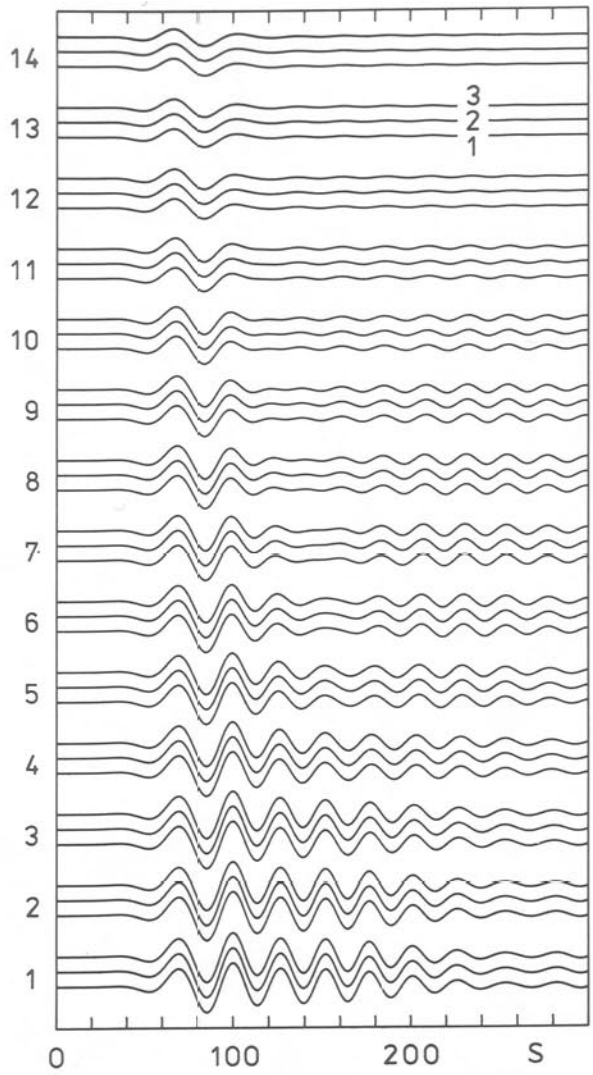

Figure 5. The seismograms for the grids 1–3 shown in Fig. 4.

the use of a fixed number of grid rows in the homogeneous basement regardless of the size of the grid spacings. In all computations in this paper six grid rows beneath the deepest point of the sediment–basement interface are used.) Grid 1 has an equidistant grid spacing and 18 grid rows. Grid 2 has an abrupt change in size of the grid spacing and 14 grid rows. Grid 3 has a gradually increasing grid spacing and 15 grid rows. The 1st and 5 bottom grid rows are not shown in Fig. 4. In between the 1st and the 2nd grid rows a zero shear modulus is assumed to simulate the free surface on the 2nd grid row. The time spacing $\Delta t = 0.1$ s is used in the computations.

The seismograms for receivers 1–14 (shown in Fig. 4) for grids 1–3 are shown in Fig. 5. The seismograms for all grids are practically the same. The very good agreement indicates that even a grid with an extremely large change in grid spacing can yield sufficiently accurate computations.

4.2 The basin with a vertical velocity gradient

Now, let us consider the basin without any internal interface (see Fig. 6). The parameters of the model are as given in

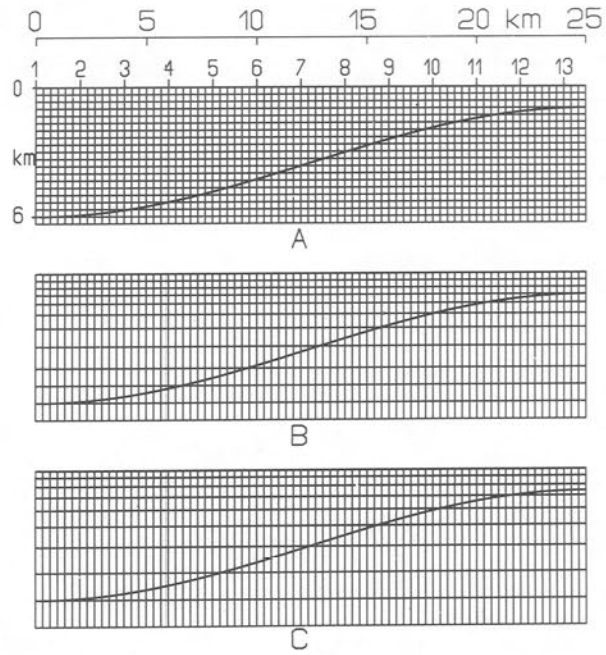

Figure 6. Parts of three grids A–C used to compute the response of the same basin model with a vertical velocity gradient. Due to the symmetry of the problem the grids only cover the right half of the basin. Numbers 1–13 denote receivers.

Table 2. The time dependence of the incident wave is given by the Ricker impulse $s(t) = (\sqrt{\pi}/2)(a - 0.5)\exp(-a)$, $a = 6(t - t_s)^2/(T_P\sqrt{6}/\pi)^2$. Here T_P is the predominant period, and the signal is defined in the interval $\langle 0, 2t_s \rangle$. In the computations $T_P = 40$ s and $t_s = 44$ s are used.

The seismograms are computed for three grids A, B, C (see Fig. 6). A total of 91 grid columns and an equidistant grid spacing of 333.3 m in the horizontal direction are used in all grids A–C. (In Fig. 6 only the 1st to the 82nd grid columns are shown.) Grids A–C differ from each other by the grid spacing in the vertical direction and thus by the number of grid points. Grid A has an equidistant grid spacing and 26 grid rows. Grids B and C have an increasing grid spacing and 18 and 16 grid rows, respectively. (Again, the 1st and 5 bottom grid rows are not shown in Fig. 6.) The grid spacings in Grids B and C satisfy the conditions (5), considering the actual velocity in corresponding depths.

Let us emphasize that the continuous linear increase of the velocity and the density inside the basin is strictly taken into account in the computations. For example, inside the basin, the vertical effective shear moduli $\mu^V_{i,j}$ are evaluated using (7). Exceptions are such vertical elements between two grid points that are crossed by the sediment–basement interface. In such a case a modified formula is used which

Table 2. Parameters of the basin shown in Fig. 6.

	S-wave velocity ($m\,s^{-1}$)	Density ($kg\,m^{-3}$)
basin:	linearly increasing	
	from	
(free surface)	200	1600
	up to	
(6 km in depth)	1200	2200
basement:	3500	3300

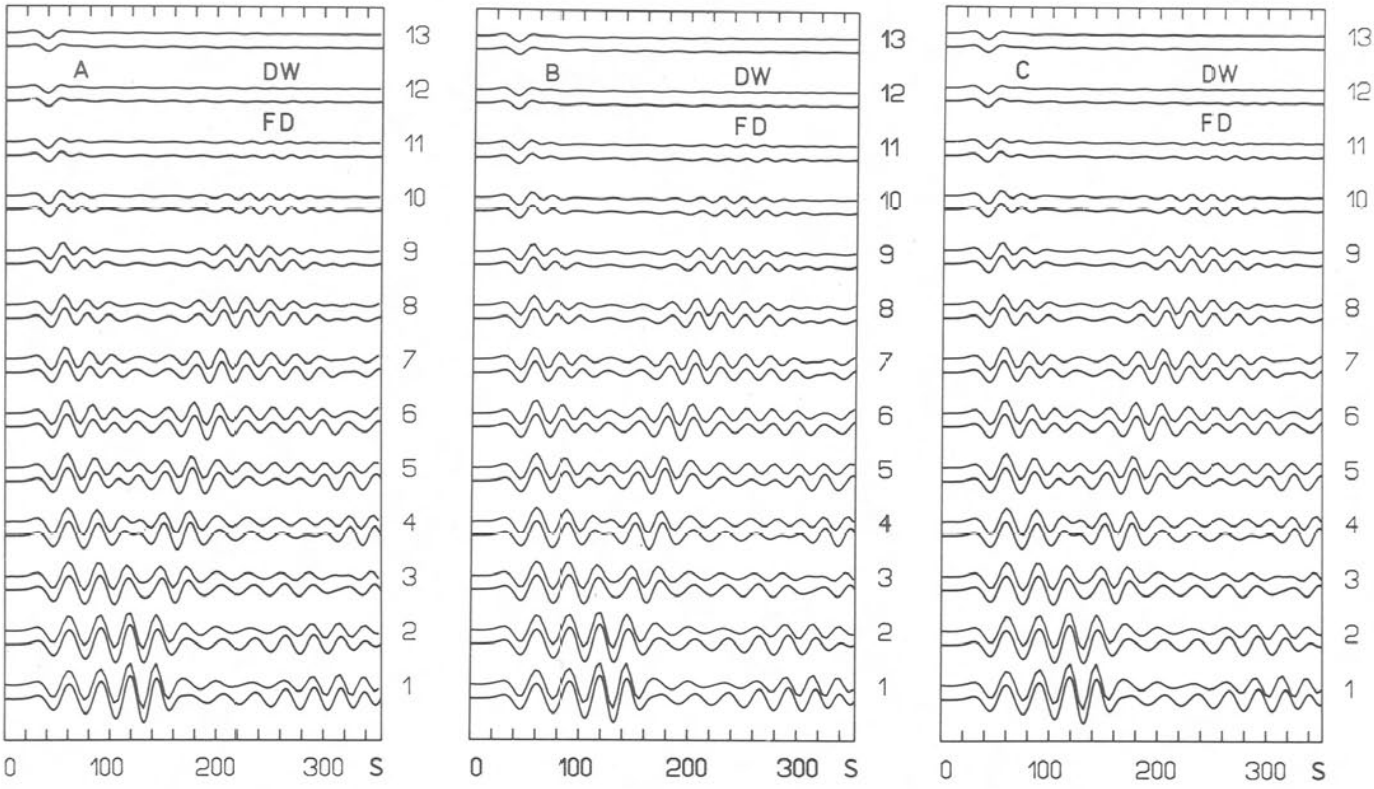

Figure 7. FD: finite-difference seismograms for the grids A, B and C shown in Figure. 6. DW: discrete-wavenumber seismograms (the same in Figs A–C) shown here for comparison. DW seismograms have been computed by P.-Y. Bard.

takes into account the interface (see equation 9). The horizontal effective shear moduli $\mu^H_{i,j}$ inside the basin are equal to actual values of μ in corresponding depths, since μ does not change in the horizontal direction. Again, exceptions are the grid points near the sediment–basement interface. The time spacing $\Delta t = 0.06$ s is used in the computations.

The seismograms for receivers 1–13 (shown in Fig. 6) for all grids are shown in Fig. 7 and they are denoted by FD. There are only insignificant differences among all FD computations. For comparison, discrete-wavenumber seismograms denoted by DW (the same in all figures A–C) are also shown in Fig. 7. Also the agreement between FD and DW seismograms is very good.

5 SEDIMENT-FILLED CHUSAL VALLEY, GARM, USSR

King & Tucker (1984) (see also Bard & Bouchon 1985) made systematic observations of the seismic response of the small (maximum 400 m wide, 700 m long), approximately 2-D sediment-filled Chusal Valley in the Garm region, USSR. The relatively deep valley exhibits a specific behaviour along transverse profiles: an in-phase motion of the valley surface, a decrease of amplitudes in the time domain from the valley centre towards the valley edge, the existence of the same fundamental resonance frequency (about 3 Hz) and a decrease of the corresponding spectral amplitudes from the valley centre towards the valley edge.

We computed *SH*-seismograms and frequency responses (transfer functions) for the central transverse profile (see King & Tucker 1984) crossing the Chusal Valley.

The total width of the valley along the profile is 376 m and the maximum depth is 60 m. The geometry of the valley is shown in Fig. 8 (refer also to Sedova 1962).

The smooth velocity–depth distribution in sediments (found by Sedova 1962) is approximated by a piece-wise linear velocity distribution (Fig. 9). The density–depth distribution is supposed in the form shown in Fig. 9. A piece-wise linear distribution is used.

The velocity and density in the basement are not known. Therefore, computations are carried out for three different basement models: (1) homogeneous basement—3500 m s^{-1} and 2800 kg m^{-3}, (2) homogeneous basement—2800 m s^{-1} and 2900 kg m^{-3}, (3) basement with a velocity gradient as inferred by Bard & Tucker (1985) and a supposed density–depth distribution as shown in Fig. 10.

The time dependence of the plane *SH*-wave incident vertically from below is given by a Gabor signal (see Section 4.1) with the predominant frequency $f_P = 3$ Hz.

A grid with 120 grid columns and 16 grid rows is used. An increasing grid spacing is used in the vertical direction. A regular grid spacing of 3.5 m in the horizontal direction is used from the left valley margin to the right one. An irregular grid spacing is used outside the valley. In Fig. 8 only the 7th to the 115th grid columns and the 2nd to the 11th grid rows are shown. The time spacing for model 1 was 0.6364 ms and for models 2 and 3 it was 0.7955 ms.

The seismograms computed for receivers 1–11 (see Fig. 8) are shown in Fig. 11. (King & Tucker 1984 recorded seismograms only for the left part of the profile from the valley edge to the site of maximum sediment thickness.) In the seismograms for all three models we can clearly see a decrease of the amplitudes from the site above the

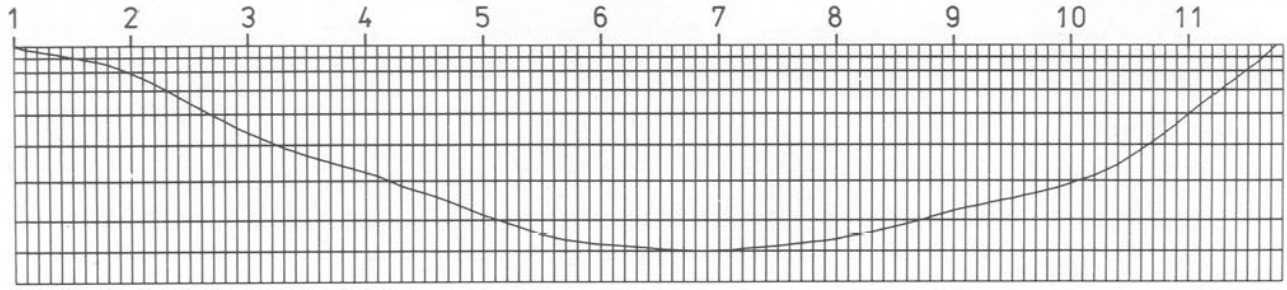

Figure 8. The geometry of the sediment–basement interface, a part of the grid used in the computations and locations of the receivers (denoted by the numbers 1–11).

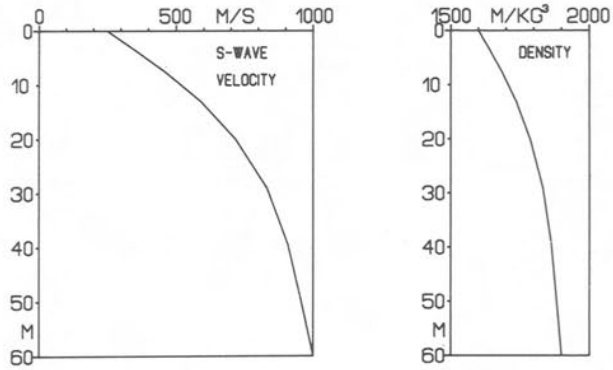

Figure 9. The piece-wise linear velocity– and density–depth distributions in valley sediments. These distributions are strictly taken into account in the computations.

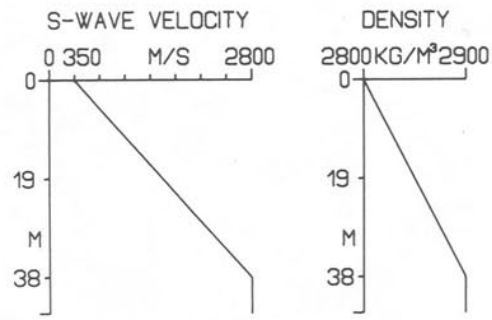

Figure 10. The velocity– and density–depth distributions in the basement of the model 3.

maximum sediment thickness (receiver 7) towards the valley edges. There is a slower decrease of amplitudes in the seismograms of receivers 3 to 1 than in those of receivers 7 to 4. Furthermore, an in-phase motion is evident mainly in the seismograms of receivers which are in positions where the sediment thickness is larger than about 40 m. These features are in qualitative agreement with the observations by King & Tucker 1984 (see fig. 7 of their paper).

The amplitudes for model 1 above the central part of the valley are larger than those for models 2 and 3.

Figure 12 shows the frequency responses, computed as ratios of amplitude spectra of the seismograms (shown in Fig. 11) and the amplitude spectrum of the signal of the incident wave. We can clearly see maxima with the same fundamental prevailing frequency of about 3.9 Hz at receivers 5 to 9. The corresponding spectral amplitudes decrease from the site above the maximum sediment thickness (receiver 7) towards the valley edges and they are larger for model 1. Besides the fundamental predominant frequency there is another one at about 5.25 Hz. There are large differences in corresponding spectral amplitudes for model 1 and for models 2 and 3, but very small differences between the responses for models 2 and 3. This means that a velocity gradient in the upper 38 m of the basement (model 3) instead of a homogeneous basement (model 2) does not significantly change the response in the frequency range considered. This can be explained by the large wavelength compared to the thickness of the velocity gradient zone.

Note that the seismograms discussed above are hardly influenced by maxima at about 5.25 Hz in the frequency responses, because the amplitude spectrum of the incident signal has its maximum at 3 Hz and effectively vanishes at about 6 Hz.

King & Tucker (1984) reported a representative fundamental predominant frequency of about 3 Hz, whereas our computations predict a frequency at 3.9 Hz. There may be several reasons for this difference. One possible explanation is that the actual velocity–depth distribution differs from that found by Sedova (1962).

6 DISCUSSION

The basins investigated in Section 4 have the lowest local velocity near the free surface along the whole extension of the model in the horizontal direction. This implies an equidistant grid spacing in this direction. (Using a varying grid spacing in such a case would yield a larger number of grid columns as compared to the equidistant spacing.) An increase of the velocity in the vertical direction allows us to use an increasing grid spacing in this direction. However, if the zone of the lowest velocity was extended from the free surface to the bottom boundary of the model it would imply an equidistant grid spacing also in the vertical direction. This shows that the usefulness of irregular grids for arbitrary 2-D models is restricted. An irregular grid is, in principle, always applicable but, in general, not always with a smaller number of grid points as compared to the regular grid.

In the case of all numerical examples presented, the use of irregular grids yields more efficient computations as compared to regular grids. It is not possible to quantify the relative efficiency in general, because this depends on the number of grid points in the regular and the irregular grid

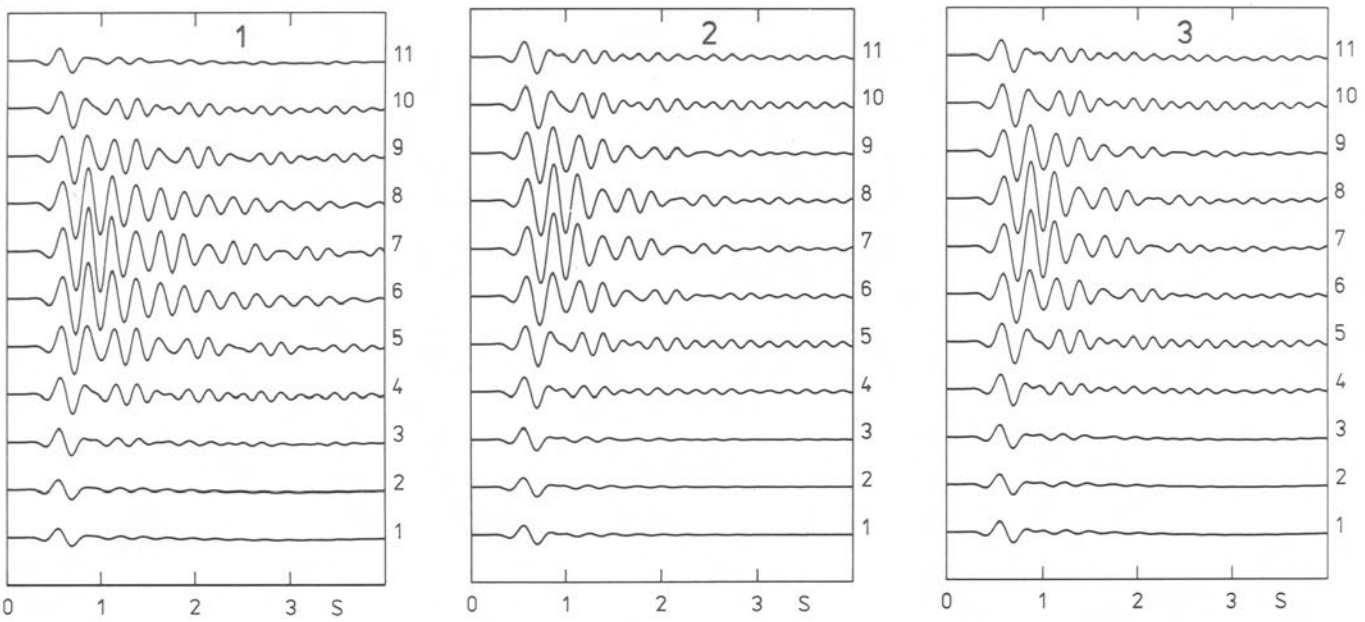

Figure 11. The seismograms for the models 1, 2 and 3 that differ from each other by the velocity and the density in the basement.

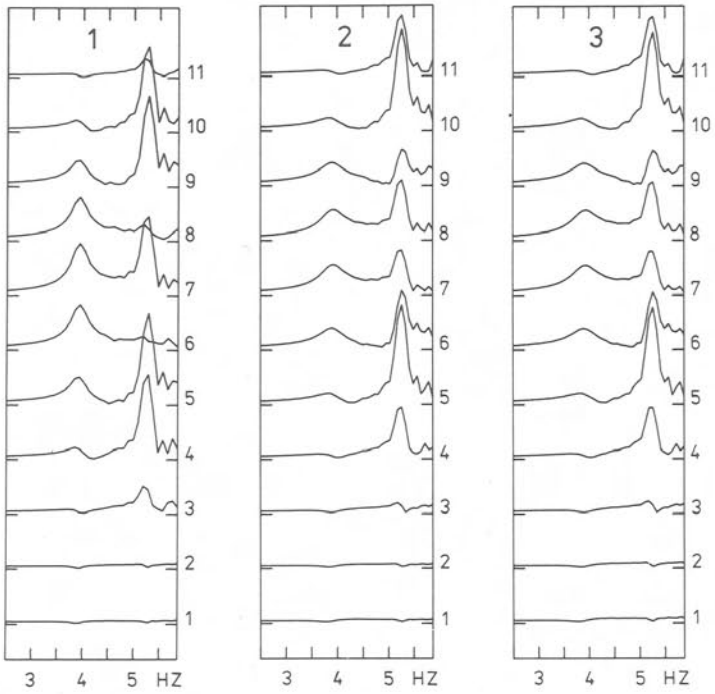

Figure 12. The frequency responses (ratios of the amplitude spectra of the seismograms shown in Fig. 11 and the amplitude spectrum of the signal of the incident wave) for the models 1, 2 and 3.

and on the model (e.g. whether the blocks of media are homogeneous or with velocity gradients).

The proposed finite-difference technique has been applied to a specific seismic response problem. However, it also can be used to solve other kinds of wave propagation problems, e.g. to compute seam waves. There, the irregular grid might be useful to model complicated fault zones of coal seams.

Absorption has not been taken into account in this paper. However, it is possible to incorporate it into the computations. In the simplest case, when the quality factor Q does not depend on spatial coordinates, the incorporation of absorption does not increase the requirements on computer time and memory, see Zahradník & Moczo (1988).

Emmerich & Korn's (1987) approach based on the rheological model of the generalized Maxwell body allows to take into account spatially dependent Q and a suitable frequency dependence. The computer time and memory increase, however, approximately twice.

7 CONCLUSIONS

A finite-difference technique is proposed which uses an irregular grid (a rectangular grid with varying spacing). The

model may be composed of blocks of media inside of which the velocity and density vary linearly in the horizontal and vertical direction. The linear velocity and density distributions are strictly taken into account in computing the effective shear moduli and the density.

The technique is applied to a specific seismic response problem in this paper. Using the example of a sedimentary basin composed of two homogeneous blocks it is shown that the regular grid, the grid with an abrupt change in grid spacing, and the grid with gradually increasing grid spacing yield practically the same results.

The seismograms computed on the free surface of a sedimentary basin with a vertical velocity gradient, using a regular grid and two irregular grids, are practically the same. They are also in very good agreement with the seismograms computed by the discrete-wavenumber method.

As an illustrative example the seismic response of the sediment-filled Chusal Valley is computed. The computations predict all main features observed by King & Tucker (1984).

In the case of all represented numerical examples the use of an irregular grid yields more efficient computations as compared to a regular grid.

ACKNOWLEDGMENTS

I am grateful to P.-Y. Bard for providing discrete-wavenumber seismograms for the basin model, to J. Zahradník and D. Majcin for helpful discussion and to V. Červený and I. Pšenčík for critically reading the manuscript. I thank the anonymous reviewers whose comments helped to improve the paper.

REFERENCES

Alterman, Z. & Karal, F. C., 1968. Propagation of elastic waves in layered media by finite-difference methods, *Bull. seism. Soc. Am.*, **58,** 367–398.

Bard, P.-Y. & Bouchon, M., 1985. The two-dimensional resonance of sediment-filled valleys, *Bull. seism. Soc. Am.*, **75,** 519–541.

Bard, P.-Y. & Tucker, B. E., 1985. Underground and ridge site effects: A comparison of observation and theory, *Bull. seism. Soc. Am.*, **75,** 905–922.

Boore, D. M., 1970. Love waves in a nonuniform waveguides: finite difference calculations, *J. geophys. Res.*, **75,** 1512–1527.

Boore, D. M., 1972. Finite-difference methods for seismic wave propagation in heterogeneous materials, in *Methods in Computational Physics,* Vol. 11, ed. Bolt, B. A., Academic Press, New York.

Boore, D. M., Larner, K. L. & Aki, K., 1971. Comparison of two independent methods for the solution of wave scattering problems: response of a sedimentary basin to vertically incident *SH*-waves, *J. geophys. Res.*, **76,** 558–569.

Emmerich, H. & Korn, M., 1987. Incorporation of attenuation into time-domain computations of seismic wave fields, *Geophysics,* **52,** 1252–1264.

Kawase, H., 1988. Time-domain response of a semicircular canyon for incident *SV, P,* and Rayleigh waves calculated by the discrete wavenumber boundary element method, *Bull. seism. Soc. Am.*, **78,** 1415–1437.

King, J. L. & Tucker, B. E., 1984. Observed variations of earthquake motion across a sediment-filled valley, *Bull. seism. Soc. Am.*, **74,** 137–151.

Korn, M., 1987. Computation of wavefields in vertically inhomogeneous media by a frequency domain finite-difference method and application to wave propagation in earth models with random velocity and density perturbations, *Geophys. J. R. astr. Soc.*, **88,** 345–377.

Mikhailenko, B. G. & Korneev, V. I., 1984. Calculation of synthetic seismograms for complex subsurface geometries by a combination of finite integral Fourier transform and finite-difference techniques, *J. Geophys.*, **54,** 195–206.

Mitchell, A. R., 1969. *Computational Methods in Partial Differential Equations,* Wiley, London.

Moczo, P., Bard, P.-Y. & Pšenčík, I., 1987. Seismic response of two-dimensional absorbing structures by the ray method, *J. Geophys.*, **62,** 38–49.

Reynolds, A. C., 1978. Boundary conditions for the numerical solution of wave propagation problems, *Geophysics,* **43,** 1099–1110.

Samarskii, A. A., 1983. *Theory of Difference Schema,* Nauka, Moscow (in Russian).

Sedova, E. N., 1962. Correlation of dynamic properties of weak earthquake records with ground conditions, *Trudi Inst. Phys. Earth, USSR,* **25,** 211–225 (in Russian).

Virieux, J., 1984. *SH*-wave propagation in heterogeneous media: Velocity-stress finite-difference method, *Geophysics,* **49,** 1933–1957.

Zahradník, J. & Moczo, P., 1988. Absorption in time-domain computations by finite-difference method, *Workshop Meeting on Seismic Waves in Laterally Inhomogeneous Media III—Abstracts,* Geophys. Inst. Czechosl. Acad. Sci., Prague.

Zahradník, J. and Hron, F., 1987. Seismic ground motion of sedimentary valleys—example La Molina, Lima, Peru, *J. Geophys.*, **62,** 31–37.